Antarctic Science 15 (1): 105–118 (2003) © Antarctic Science Ltd Printed in the UK DOI: 10.1017/S095410200300110X

An optimum multiparameter mixing analysis of the shelf waters in the Ross Sea

G. BUDILLON[1]*, M. PACCIARONI[1], S. COZZI[2], P. RIVARO[3], G. CATALANO[2], C. IANNI[3] and C. CANTONI[2]

[1]*Università di Napoli "Parthenope", Istituto di Meteorologia e Oceanografia, Via De Gasperi 5, 80133 Napoli, Italy*
[2]*Consiglio Nazionale delle Ricerche, Istituto Sperimentale Talassografico, Via Gelsi 2, 34123 Trieste, Italy*
[3]*Università di Genova, Dipartimento di Chimica e Chimica Industriale, Via Dodecanneso 31, 16146 Genova, Italy*
**giorgio.budillon@uninav.it*

Abstract: The analysis of the mixing processes involving water masses on the Ross Sea continental shelf is one of the goals of the CLIMA project (Climatic Long-term Interactions for the Mass balance in Antarctica). This paper uses extended Optimum MultiParameter analysis (OMP), which is applied to four datasets collected during the cruises of 1994/95, 1995/96, 1997/98 and 2000/01 in the Ross Sea (Antarctica). Data include both hydrological, (temperature, salinity, and pressure; T, S, and P, respectively) and chemical parameters (O_2, $Si(OH)_4$, PO_4, and NO_3+NO_2). The OMP analysis is based on the assumption that the mixing is a linear process which affects all parameters equally so that each sample shows physical/chemical properties that are the result of the mixing of some properly selected Source Water Types (SWTs). OMP thus evaluates the best set of contributions by all SWTs to each sample, and allows the spatial distribution and structure of the water masses in a basin to be evaluated. Ocean circulation may subsequently be inferred by means of a deeper analysis of the spreading of the water mass. In this study, the "real" Redfield ratios observed in the Ross Sea were used to correct the equations referring to the chemical parameters in accordance with the extended version of OMP. The solutions include some physically realistic constraints. The results allow a detailed description of the water mass distribution, validated through comparison with some "canonical" thermohaline characteristics of the Ross Sea hydrology. In particular our results verify the spreading of the HSSW over the entire continental shelf and emphasize the key role it plays in the ventilation of the deep waters outside the Ross Sea. In addition a description is given of the intrusion of relatively warm waters coming from the open ocean and flowing at some specific locations at the continental shelf break.

Received 13 February 2002, accepted 23 October 2002

Key words: Antarctic, circulation, continental shelf, OMP, water masses,

Introduction

During the last few decades, the water masses comprising Ross Sea have been the object of several investigations (Jacobs *et al*. 1985, Locarnini 1994, Jacobs & Giulivi 1998, Gordon *et al*. 2000), but no complete and clear description of their distribution in this area is yet available. This study aims to investigate the mixing of the main water masses identified on the Ross Sea continental shelf, in order to understand better their circulation, particularly in the intermediate and deep layers of the basin.

This analysis is based on the dataset collected during four cruises, from 1994 to 2001, as part of the CLIMA project (Climatic Long-term Interaction for the Mass balance in Antarctica), supported by the Italian National Research Program in Antarctica (PNRA). Hydrological and chemical data were processed using the method of extended Optimum MultiParameter (OMP) analysis, to provide a more detailed description of water masses in the Ross Sea. The results constitute the first application of this method in the Antarctic seas and are validated through comparison with observations of the classical thermohaline properties observed in the Ross Sea.

The OMP method was introduced by Tomczak (1981) and further developed by Mackas *et al*. (1987) and Tomczak & Large (1989) as a tool for evaluating the spatial distribution of the oceanic water masses and for inferring information regarding their circulation. It uses both physical (temperature and salinity) and chemical (nutrients and dissolved oxygen or other chemical tracers) data to calculate the contributions – in an objectively definable best fit – of well identified source water types (SWTs) to each sample, in order to match the field observations. Some physically realistic constraints are included: the contribution from all SWTs must add up to 100% and all SWTs contributions must be non-negative.

Physical background

The Ross Sea sits over the Antarctic continental shelf between the longitudes 164°E and 164°W. It covers an area of about 5 x 10^5 km^2 and has an average depth of *c.* 500 m with a rather irregular bottom topography characterized by several banks and depressions down to a depth of 1200 m. The continental shelf break, which corresponds to the 700 m

isobath, runs NW–SE and links the area in front of Cape Adare to Cape Colbeck. Some depressions in the inner area are deeper than the continental shelf break, and therefore behave as reservoirs of the salty and dense waters.

The Circumpolar Deep Water (CDW) is carried by the Antarctic Circumpolar Current (ACC) along the boundary of the Ross Sea, following the shelf slope from east to west. CDW strongly influences the thermohaline circulation of this basin, being the only water mass which provides heat to the shelf waters (Jacobs *et al*. 1985, Locarnini 1994, Jacobs & Giulivi 1998, 1999, Gouretsky 1999, Budillon *et al*. 2000). In some specific locations it intrudes onto the Ross continental shelf forming, after the interaction with the shelf waters, the modified CDW (MCDW), which can be identified by a subsurface maximum temperature and minimum dissolved oxygen (Jacobs *et al*. 1985, Locarnini 1994, Budillon *et al*. 1999).

On the western side of the Ross Sea, the physical features of the water column are also affected by the recurring presence of a substantial coastal ice free area, the Terra Nova Bay polynya (Bromwich & Kurtz 1984, Jacobs *et al*. 1985, Budillon & Spezie 2000, Fusco *et al*. 2003). This region has been identified as the area where the High Salinity Shelf Water (HSSW) is generated by the continual formation and removal of new ice, which increases seawater salinity (Kurtz & Bromwich 1983, 1985, Jacobs *et al*. 1985, Van Woert 1999). As a result of this processes, the Ross Sea displays a negative W–E gradient of the salinity and density fields and a massive presence of the HSSW in the deeper layers of its western side. The HSSW spreads close to the bottom, following the axis of the Drygalski Basin in both north and south directions. The northward branch of HSSW reaches the continental shelf break where it mixes with the MCDW forming deep and bottom waters (Jacobs *et al*. 1970, Gordon & Tchernia 1972, Rodman & Gordon 1982, Budillon *et al*. 1999). The southerly branch of HSSW, after reaching the end of the Drygalski Basin, is believed to move beneath the Ross Ice Shelf where it interacts with the basal ice (Jacobs *et al*. 1979). When it flows out, HSSW is modified into Deep Ice Shelf Water (DISW), which is colder than the surface freezing point, as well as fresher and less dense (Jacobs *et al*. 1979, 1985, 1989, Jacobs & Comiso 1989, Trumbore *et al*. 1991, Locarnini 1994, Bergamasco *et al*. 2002). The DISW core is located at an intermediate depth (from 300–500 m) and moves northward along the Challenger Basin (Budillon *et al*. 2002, Rubino *et al*. 2003). When the DISW reaches the continental shelf break of the Ross Sea, it mixes with the MCDW, making a further contribution to the formation of deep and bottom waters in the Southern Ocean (Jacobs *et al*. 1985, Trumbore *et al*. 1991). Because of these processes, HSSW and DISW are the most important shelf waters of the Ross Sea involved in the deep ocean ventilation.

A further water mass is the Low Salinity Shelf Water (LSSW) which is massively present at intermediate depths in the central eastern Ross Sea (Jacobs *et al*. 1985, Locarnini 1994, Russo 1999). Its formation appears to be due to the interaction between Antarctic Surface Water (AASW) and colder waters in the subsurface layers, after several freezing (melting) cycles of the surface water (ice) (Jacobs *et al*. 1985). The AASW is observed mainly in the mixed layer (20–100 m) during summer. It derives from the upwelled and modified CDW (Jacobs *et al*. 1985) after mixing with underlying waters, which have a relatively lower temperature and a salinity below 34. The AASW behaviour is extremely variable in the course of the year, being influenced by atmospheric conditions, ice melting and formation, and precipitation (Jacobs *et al*. 1985). When massive melting of pack ice occurs, the large freshwater advection further decreases the AASW salinity to < 33, generating a very stable upper mixed layer. Moreover, this process also releases into the upper ocean nutrient and micro-elements of meteoric origin that have been entrapped in the pack ice during winter (Grotti *et al*. 2001, Ianni *et al*. in press). For these reasons, the presence of AASW favours the onset of intense phytoplankton blooms and has often been associated with events of increased primary productivity. In this work the AASW has been incorporated into the SWT definitions to provide more information for resolving the system. However, due to large short-term changes (in time and space), no certain results regarding its spreading are yet available. Consequently, only the results regarding subsurface layers have been reported and discussed here.

Material and methods

The CLIMA project cruises were carried out in the Ross Sea by the RV *Italia*, during the summer of the years 1994/95, 1995/96, 1997/98 and 2000/01. Hydrographical data (depth, temperature and salinity) were collected using a multiparameter CTD probe (SBE 9/11 plus) equipped with two temperature and two conductivity sensors and with a SBE Carousel water sampler. CTD salinity acquisitions were calibrated using salinometer analyses of bottle samples collected at each station and at several depths. The CTD records worked at the highest frequency allowed by the probes (24 Hz), spanning the water column from the surface to a nominal depth of 1 m above the bottom. They were subsequently processed following standard procedures and algorithms (UNESCO 1983, 1988).

Samples for salinity, dissolved oxygen and nutrients (silica, nitrate plus nitrite and phosphate) analysis were taken using 24 x 10 l Niskin bottles fitted to the SBE Carousel. All water samples were collected during the up-cast.

Dissolved oxygen was determined according to the Winkler method (Strickland & Parsons 1972), modified with potentiometric detection of the end point.

During the 1994/95 and 1995/96 cruises, nutrient

https://doi.org/10.1017/S095410200300110X Published online by Cambridge University Press

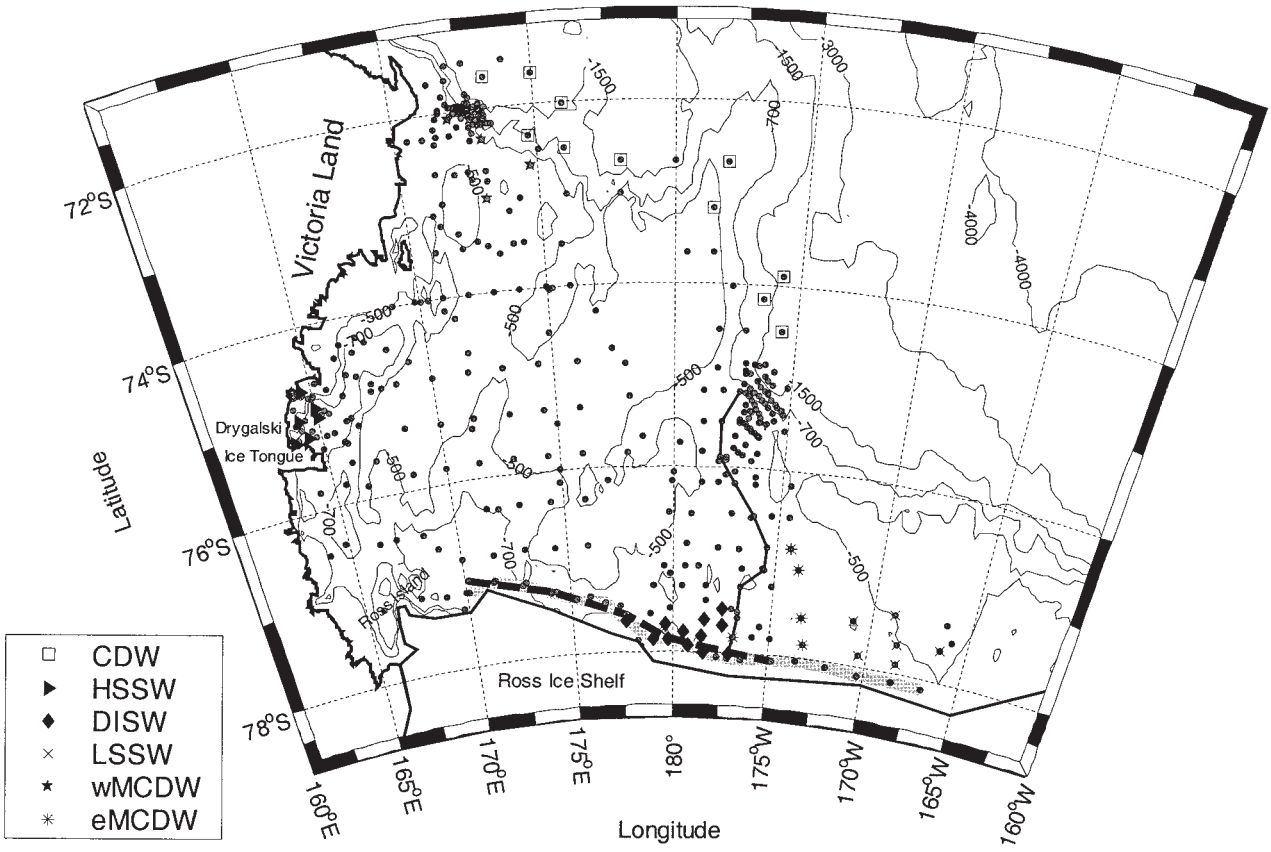

Fig. 1. Position of the CTD stations occupied during the four cruises. The solid gray line, the dashed black line, and solid line denote stations used for the vertical sections of Figs 3, 4 & 5, respectively. Hydrographical stations used for the water mass definitions are also indicated using the symbols shown in the legend.

concentrations were determined directly on board using the segmented flow colorimetric technique, applied on both Alpkem (Alpkem 1992a, 1992b, 1992c) and Technicon II autoanalysers (Hansen & Grasshoff 1983). On the 1997/98 and 2000/01 cruises, water samples were filtered through GF/F filters immediately after collection and stored at -30°C in 100 ml low density polyethylene containers until analysed. Samples were then thawed in a tepid water bath and analysed on a Technicon II autoanalyser. All chemical concentrations used in the numerical computations of this paper are expressed in $\mu mol \cdot dm^{-3}$.

Optimum Multiparameter (OMP) analysis

The basic assumption of OMP analysis is that a linear relationship exists between the parameters. This entails considering complete mixing so that all turbulent coefficients can be considered as being of the same order. The most important step in this analysis is to express all seawater samples as linear combinations of some selected sea water types (SWTs), whose physical and chemical properties are fully known (http://www.ldeo.columbia.edu/~jkarsten/omp_std, Poole & Tomczak 1999).

Although a water mass can be represented as a combination of an infinite number of SWTs, some ocean regions, in which a single water mass is found, distinctly show linear relationships between temperature and salinity, so that two SWTs can be considered to represent the water mass. In some cases, when a water mass is the result of a very localized formation process, it can be represented by a single SWT (e.g. Tomckaz 1999) in the vicinity of the formation region. The parameters are identified with average values and standard deviations, which depend on the environmental variability and the accuracy of the measurement. When defining the SWT, literature values can also be used. For the Ross Sea, Jacobs *et al*. (1985) and Trumbore *et al*. (1991) provide the starting points for the definition of the water masses in terms of depth, salinity, temperature and dissolved oxygen. In this study we used Jacobs *et al*.'s (1985) definitions in order to identify the presence of the water masses in our dataset relevant to this study and to localize their associated source regions. For each of them, scatter plots of potential temperature against salinity were produced and refined by removing the observations at the boundary.

MCDW requires a different approach because it intrudes

https://doi.org/10.1017/S095410200300110X Published online by Cambridge University Press

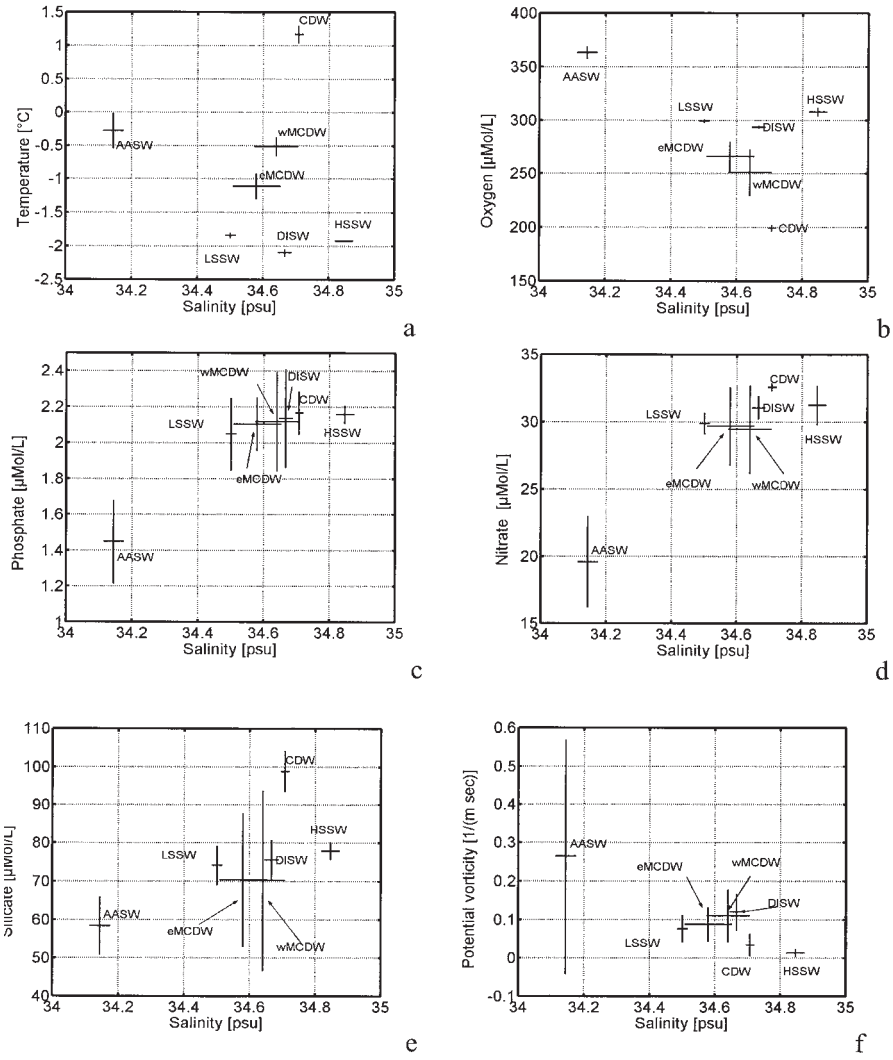

Fig. 2. Water mass definition values for the AASW (Antarctic Surface Water), CDW (Circumpolar Deep Water), MCDW (Modified Circumpolar Deep Water), LSSW (Low Salinity Shelf Water), DISW (Deep Ice Shelf Water), and HSSW (High Salinity Shelf Water) used as SWT for this study.

on the continental shelf at specific locations in both the eastern and western Ross Sea, and takes on slightly different thermohaline characteristics depending on its interaction with the other water masses (Budillon *et al*. 1999). Therefore, in this study, two water mass types are used as a compromise to define MCDW: western MCDW and eastern MCDW (wMCDW and eMCDW, respectively). This takes into account the different pathways and mixing processes involved in MCDW.

All these considerations were taken into account in order to identify the source regions of each water mass (Fig. 1) and their physical parameters. This *modus operandi* introduces a degree of subjectivity in the water mass definitions; however it represents a good compromise and minimizes the influence of other water masses and biological processes in each water mass definition.

Table I. Water mass definitions (modified from Jacobs *et al*. 1985), Redfield ratios, and weighting used in the OMP analysis for this study.

Sea water type	CDW	AASW	DISW	wMCDW	eMCDW	LSSW	HSSW	Redfield ratio	Weighting
Parameter									
Potential Temperature (°C)	1.70	-0.50	-2.21	-0.40	-1.30	-1.80	-1.92	-	25
Salinity	34.73	34.00	34.62	34.52	34.50	34.47	34.88	-	25
Oxygen (µmol dm^{-3})	191	370	298	230	279	300	298	-100	8
Phosphate (µmol dm^{-3})	2.1	1.2	2.2	2.2	2.1	2.1	2.2	1	1
Nitrate (µmol dm^{-3})	32.7	23.0	31.7	32.1	30.0	29.0	31.0	12	0.5
Silicate (µmol dm^{-3})	120.0	58.0	79.0	89.0	78.0	76.0	80.0	25	1
Potential vorticity (m^{-1} sec^{-1}) x 10^8	0.008	0.200	0.100	0.005	0.080	0.075	0.001	-	2
Mass conservation	-	-	-	-	-	-	-	-	25

https://doi.org/10.1017/S095410200300110X Published online by Cambridge University Press

Analysis of the depth, temperature and salinity ranges in each source region considered in this study allow the definition of the source water type in parameter space. First, the potential temperature and salinity values were determined for each sea water type and these data were used in linear regression computation to estimate the values of the other chemical properties. Together with salinity and potential temperature, these values constituted the source water mass definitions.

Scatter plots of dissolved oxygen, nitrate plus nitrite, phosphate, and silicate as well as of the potential vorticity against salinity were produced for the definition of the value ranges for the chemical parameters of each water type. The observed parameters are plotted in Fig. 2, and the regression results are shown in Table I along with the weighting for each hydrographical variable. These values (which are slightly different from those found in Jacobs *et al*. (1985)) have been used for defining the SWTs.

The extended version of OMP (Tomczak & Large 1989, Kartensen & Tomczak 1998) has been used in this study, taking into account, as tracers, seven parameters: potential temperature (°C), salinity (psu), oxygen (μmol dm^{-3}), phosphate (μmol dm^{-3}), nitrate + nitrite (μmol dm^{-3}), silicate (μmol dm^{-3}), and potential vorticity (m^{-1} s^{-1}). Potential vorticity is conserved below the mixed layer, when the flow field is assumed to be in quasi-geostrophic equilibrium. Therefore, it can be considered as a conservative tracer of the equation system (http://www.ldeo.columbia.edu/~jkarsten/omp_std). Potential vorticity is essential for the propagation of information modelling in the ocean. Even though it is a dynamical quantity, it is a useful tracer of flow since it has identifiable sources and sinks, and is complementary to other properties such as salinity, nutrients and chemical tracers. Unlike the other parameters, which are measured, potential vorticity is calculated using the formula:

$$PotVorticity = N^2 \frac{f}{g}$$

where N is the Brunt-Väisälä frequency (s^{-1}), f the Coriolis term (s^{-1}), and g the gravity (m s^{-2}). The inclusion of potential vorticity as a tracer in the OMP analysis adds a new dynamic constraint.

In the case of the extended version of OMP analysis, the chemical parameters (i.e. nutrients) are also included in order to extend the number of possible SWTs. Since these parameters can be modified in the marine environment by non-conservative processes (biological uptake or remineralization), the change of concentration due to biogeochemical reactivity is expressed, in the case of phosphate, as an unknown ΔP quantity. In the other cases, the Δ nutrient is calculated with respect to ΔP using the Redfield ratios as coefficients for conversion between phosphorus and oxygen, nitrogen and silicon.

Due to the structural role of nitrogen and phosphorus in the physiology of phytoplankton cells and to their comparable turn-over time, the assimilation N/P ratio is nearly constant for large scale ecosystems. In the Ross Sea this ratio has been evaluated using different approaches as 11.3 ± 3.6 (Catalano *et al*. 1997) or 11.0 ± 0.3 (Saggiomo *et al*. 2002), i.e. slightly lower than the classical value of 16 (Redfield *et al*. 1963). However, it is well inside the range of 9.5–19 found by several researchers in the Antarctic seas (El-Sayed & Taguchi 1981, Jennings *et al*. 1984, Le Jehan & Treguer 1985, Arrigo *et al*. 1999). Some of these authors argue that this range of values is due to the different ability of Antarctic phytoplankton to incorporate phosphorus into its "energy cycle" (e.g. ATP, adenosinetriphosphate, and ADP, adenosinediphosphate). Still others believe that it depends on the differing structures of phytoplankton communities.

The value of the Si/N, and therefore of the Si/P, ratio, is less constant than N/P because silicon is structural only for diatom cells, which need it for their silica exoskeleton. Large variations in Si/N thus occur in the Ross Sea depending on the predominance of diatoms or *Phaeocystis antarctica* in the blooms. From the data collected in the Ross Sea during the 1995–96 cruise, the Si/N disappearance ratio was estimated to be 1.9 ± 0.1 when little or no sea ice melting water was present in the euphotic layer (salinity ≥ 34.1). In contrast, when sea ice melt water was massively present in the upper part of the water column (salinity down to 33.0), the Si/N ratio rose to 2.2 ± 0.1. However, in particular zones like Terra Nova Bay, when contemporary fresh water presence and diatom bloom occurred, values of Si/N ratio as high as 3.4 were also found (Catalano *et al*. 1997, 1999).

In order to establish a value for the O_2/P ratio suitable for use in OMP analysis of the Ross Sea, a better approximation can be derived, in our opinion, from the coefficients of the Redfield equation (Redfield *et al*. 1963). Therefore, the O_2/P ratio can be theoretically assessed at 138 or 107 for systems respectively characterized by predominant "new production" or "recycled production". Taking into consideration the *f*-ratio (Eppley & Peterson 1979) to discern predominance between "new" and "regenerated" production, both marginal ice zones and open waters of the Ross Sea seem to be characterized in January–February (Nelson & Smith 1986, Lipizer *et al*. 1997, 2000) by a predominant "new" production (*f*-ratio ≈ 0.7).

As mentioned previously, AASW, CDW, DISW, HSSW, LSSW, and MCDW are considered in this study. The last is composed of two different water mass definitions to account for the distinct characteristics in the western and eastern sectors. Given these definitions, the SWT's parameters are arranged in the following matrix (G). The contribution of each SWT to a dataset point is represented by the vector X. The observed parameters at each point are in the vector B and the R vector represents the residuals, which have to be minimized in the solution of the analysis

https://doi.org/10.1017/S095410200300110X Published online by Cambridge University Press

in the last square sense.

The general system in matrix notation is:

$$\begin{bmatrix} \theta_1 & \theta_2 & \theta_3 & \theta_4 & \theta_5 & \theta_6 & \theta_7 & 0 \\ S_1 & S_2 & S_3 & S_4 & S_5 & S_6 & S_7 & 0 \\ O_1 & O_2 & O_3 & O_4 & O_5 & O_6 & O_7 & -r\frac{O}{P} \\ P_1 & P_2 & P_3 & P_4 & P_5 & P_6 & P_7 & 1 \\ N_1 & N_2 & N_3 & N_4 & N_5 & N_6 & N_7 & r\frac{N}{P} \\ Si_1 & Si_2 & Si_3 & Si_4 & Si_5 & Si_6 & Si_7 & r\frac{Si}{P} \\ Pv_1 & Pv_2 & Pv_3 & Pv_4 & Pv_5 & Pv_6 & Pv_7 & 0 \\ 1 & 1 & 1 & 1 & 1 & 1 & 1 & 0 \end{bmatrix} \begin{bmatrix} x_1 \\ x_2 \\ x_3 \\ x_4 \\ x_5 \\ x_6 \\ x_7 \\ \Delta\rho \end{bmatrix} = \begin{bmatrix} \theta_{obs} \\ S_{obs} \\ O_{obs} \\ P_{obs} \\ N_{obs} \\ Si_{obs} \\ Pv_{obs} \\ 1 \end{bmatrix} + \begin{bmatrix} R_\theta \\ R_S \\ R_O \\ R_P \\ R_N \\ R_{Si} \\ R_{PV} \\ R_{mass} \end{bmatrix}$$

(G) (X) = (B) + (R)

The last row accounts for mass conservation, since the sum of each water type has to reach unity. Each column (j goes from 1 to 7) corresponds to a SWT which is a point in the parameter space with coordinates θ_j, S_j, O_j, P_j, N_j, Si_j, P_j. If this point belongs to a source region (as it occurs in a preliminary definition step) it is defined as a Source Water Type. The terms

$$r\frac{O}{P}, \qquad r\frac{N}{P}, \qquad r\frac{Si}{P}$$

indicate the Redfield ratios for oxygen, nitrate, and silicate versus the phosphate.

Vector B, the matrix G and the Redfield ratios are normalized in order to make the parameters nondimensional, and comparable:

$$\mathbf{B}'_{\mathbf{i}} = (\mathbf{B}_{\mathbf{j}} - \overline{\mathbf{G}}_{\mathbf{i}})/\delta_{\mathbf{i}}$$

$$\mathbf{G}'_{\mathbf{i,j}} = (\mathbf{G}_{\mathbf{i,j}} - \overline{\mathbf{G}}_{\mathbf{i}})\delta_{\mathbf{i}}$$

In which:

$$\delta_{\mathbf{i}} = \sqrt{\frac{1}{n}\sum_{j=1}^{n}(\mathbf{G}_{\mathbf{i,j}} - \overline{\mathbf{G}}_{\mathbf{i}})^2}$$

with

$$\overline{\mathrm{G}}_{\mathrm{i}} = \frac{1}{n}\sum_{j=1}^{n} G_{i,j}$$

To normalize the Redfield ratios:

$$r'_{tracer/P} = \frac{(G'_i)_{\max} - (G'_i)_{\min}}{(G_i)_{\max} - (G_i)_{\min}} r_{tracer/P}$$

Finally the system's rows are weighted according to the Tomczak (1999) formula:

$$W_i = \frac{\sigma_i^2}{\delta_i(\max)}$$

where

$$\delta_{\mathbf{i}} = \sqrt{\frac{1}{n}\sum_{j=1}^{n}(\mathbf{G}_{\mathbf{i,j}} - \overline{\mathbf{G}}_{\mathbf{i}})^2}$$

Here δ_i is a measure of the suitability of parameter "i" for resolving the difference in water mass content (Tomczak 1989) and δ_i is the largest variance for parameter "i" among all SWTs.

Results and discussion

The results obtained from the mixing model are shown as patterns of the water masses along vertical and horizontal sections in Figs 3–9. Mass conservation residuals were also computed by OMP. Since the equations are normalized, their values afford an objective evaluation of the quality of the solutions. A low (high) residual indicates that the properties of the samples are well (poorly) represented by the set of SWTs considered. The upper limit of the mass conservation residuals can be used to identify and to remove the regions poorly described by the mixing of the SWTs, where the environmental variability and/or the measurement errors make the results of the analysis uncertain. In this work, we chose a value of 5% (Poole & Tomczak 1999) and only the results with mass conservation residuals below this limit are shown. Moreover, as a further constraint, only areas where a single water type has > 40% plotted (Figs 3–9).

Figures 3 & 4 show the results of the model along the RIS during two successive surveys (summers 1994/95 and 1995/96, respectively). Since the water mass distribution along the RIS has been described in detail in several papers (e.g. Jacobs *et al*. 1985, Trumbore *et al*. 1991, Jacobs & Giulivi 1999), this region was used in this study to validate our results. Despite any differences due to variable conditions during the sampling (owing to the presence of sea ice, no stations were occupied further east during the 1996/97 survey), they allow of a qualitative comparison between the two observation periods.

The contributions of HSSW, DISW, LSSW, and MCDW along the RIS are shown in Fig. 3 (summer 1994/95) and Fig. 4 (summer 1995/96). These longitudinal sections adequately represent the general distribution of sub-thermocline water masses. The west–east decreasing gradient of HSSW is well represented by the results shown in Figs 3d & 4d. On the western side of the RIS, the bottom layer is filled by HSSW up to the longitude of 175°W, where its spread is limited by the eastern flank of Ross Bank. In this area, HSSW constitutes more than 50% of seawater volume at depths > 200 m. A remarkable difference is found comparing Figs 3d & 4d. The HSSW concentration percentage between 175°E and 175°W is found at a depth range of between 400–500 m during the summer 1994/95 (Fig. 3d) while one year later the same

https://doi.org/10.1017/S095410200300110X Published online by Cambridge University Press

HSSW concentration is found at deeper levels (Fig. 4d).

A decrease in HSSW concentration is in agreement with the water freshening recently observed by Jacobs & Giulivi (1998, 1999) in the western sector of the Ross Sea and by Budillon & Spezie (2000) in the coastal area of Terra Nova Bay. Moreover a general freshening of the shelf waters (with different magnitudes) has been observed in the Ross Sea and environment. This freshening appears to be the result of a combination of different forcings, which include increased precipitation, a decreased sea ice production, and an increased melting of the Western Sea Ice Sheet (Jacobs *et al*. 2002).

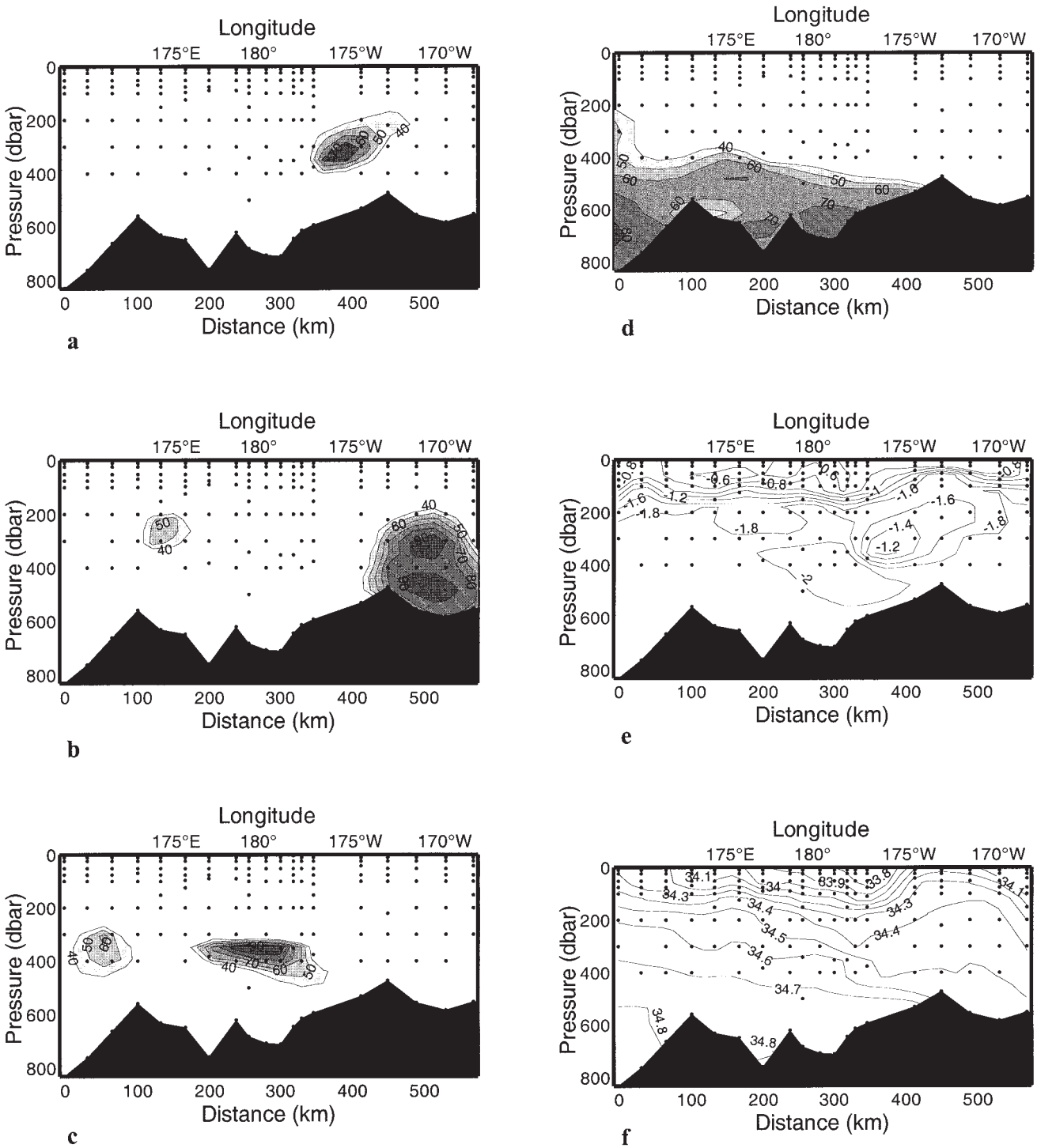

Fig. 3. OMP analysis solutions along a vertical section close to the RIS (Ross Ice Shelf) (see Fig. 1) during summer 1994/95; showing **a.** MCDW, **b.** LSSW, **c.** DISW, **d.** HSSW contributions, **e.** potential temperature along the section, **f.** salinity fields along the section.

https://doi.org/10.1017/S095410200300110X Published online by Cambridge University Press

Above this layer, a considerable southward penetration of MCDW occurs at a depth of 300 m in Fig. 3a and is hinted at in Fig. 4a. At approximately the same depth, but shifted toward the west, the northward flowing DISW is evident in Figs 3c & 4c. The area occupied by the DISW maximum contribution was found to be located at approximately the same geographic position during the two surveys, corresponding to the outflow region previously identified in previous works (e.g. Jacobs *et al*. 1985). The area occupied by the DISW appears larger and deeper in 1995/96 than in 1994/95 probably due to a lesser influence of the HSSW in the first cruise.

LSSW appears to be massively present in the eastern sector from 300 m to the bottom, in the summer 1994/95

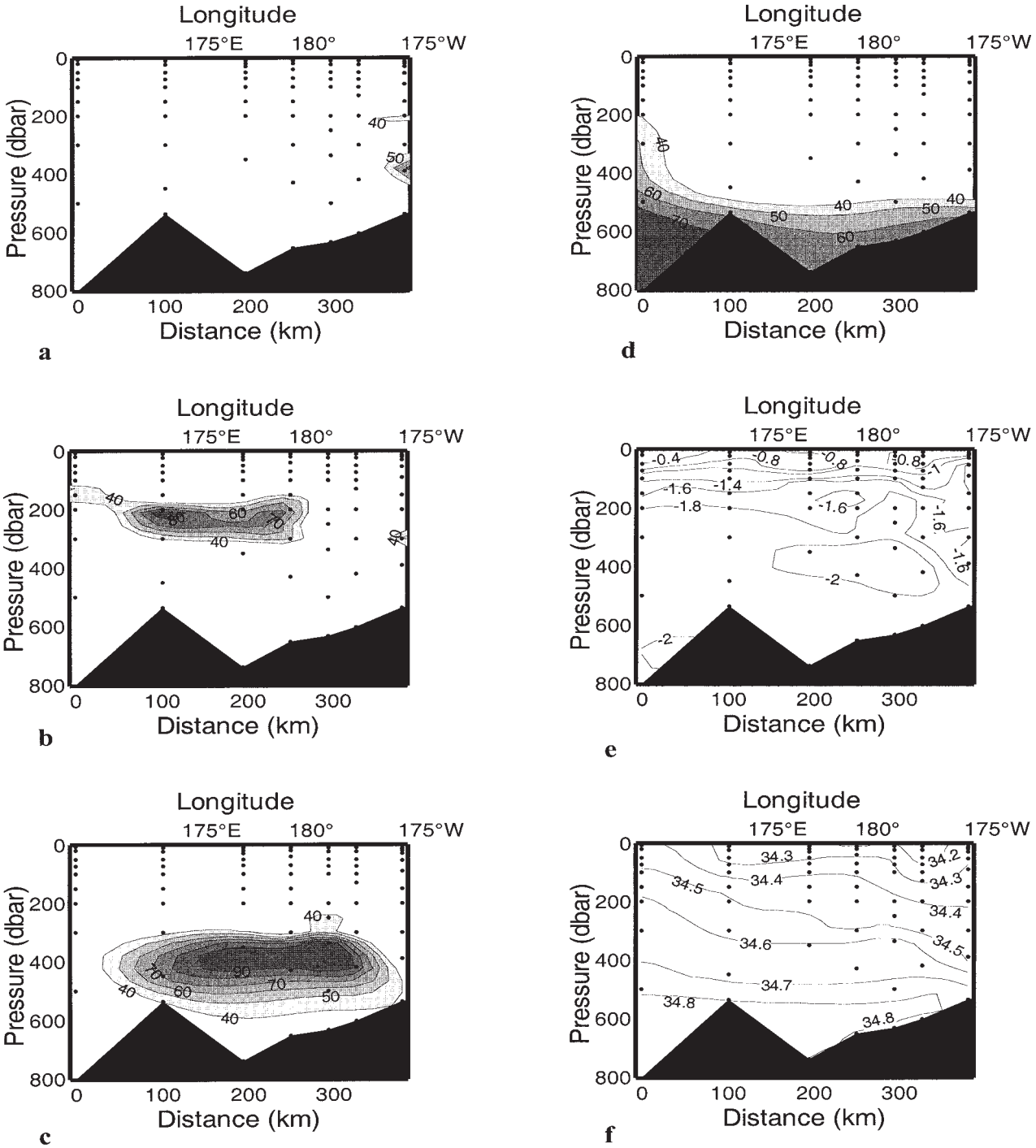

Fig. 4. OMP analysis solutions along a vertical section close to the RIS (Ross Ice Shelf) (see Fig. 1) during summer 1995/96; showing **a.** MCDW, **b.** LSSW, **c.** DISW, **d.** HSSW contributions, **e.** potential temperature along the section, **f.** salinity fields along the section.

https://doi.org/10.1017/S095410200300110X Published online by Cambridge University Press

(Fig. 3b); the incomplete sampling during 1995/96 precludes its observation during that field season. As shown in Figs 3b & 4b it becomes an intermediate water mass in the western sector where it is found at a depth of 300 m.

Interactions between MCDW, LSSW, DISW, and HSSW along the continental shelf are shown more clearly in Fig. 5, which illustrates the results of the model along a section linking the RIS to the continental slope at about 178°W (see

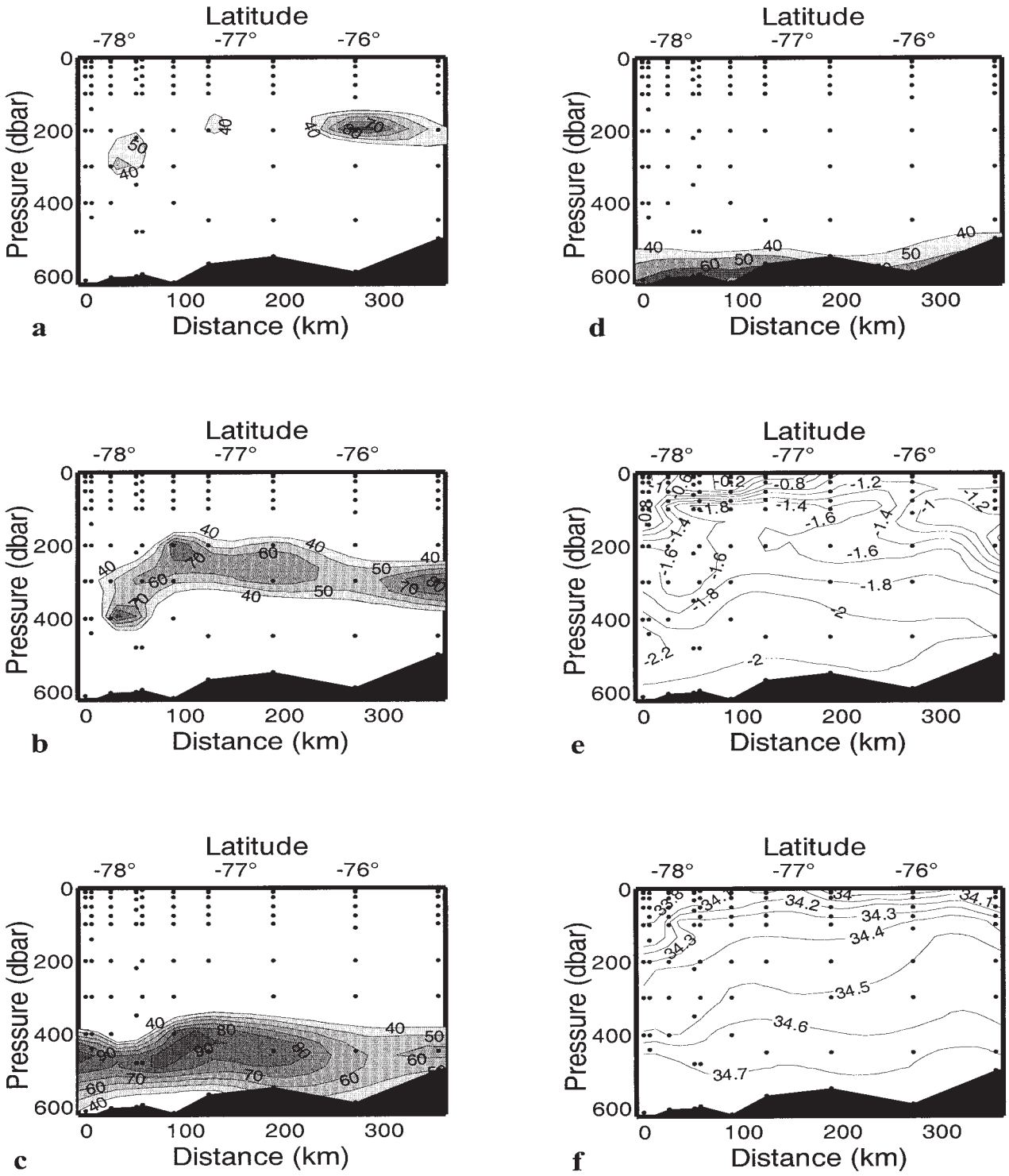

Fig. 5. OMP analysis solutions along a vertical section between the RIS (Ross Ice Shelf) and the continental slope (see Fig. 1) during summer 1994/95; showing **a.** MCDW, **b.** LSSW, **c.** DISW, **d.** HSSW contributions, **e.** potential temperature along the section, **f.** salinity fields along the section.

https://doi.org/10.1017/S095410200300110X Published online by Cambridge University Press

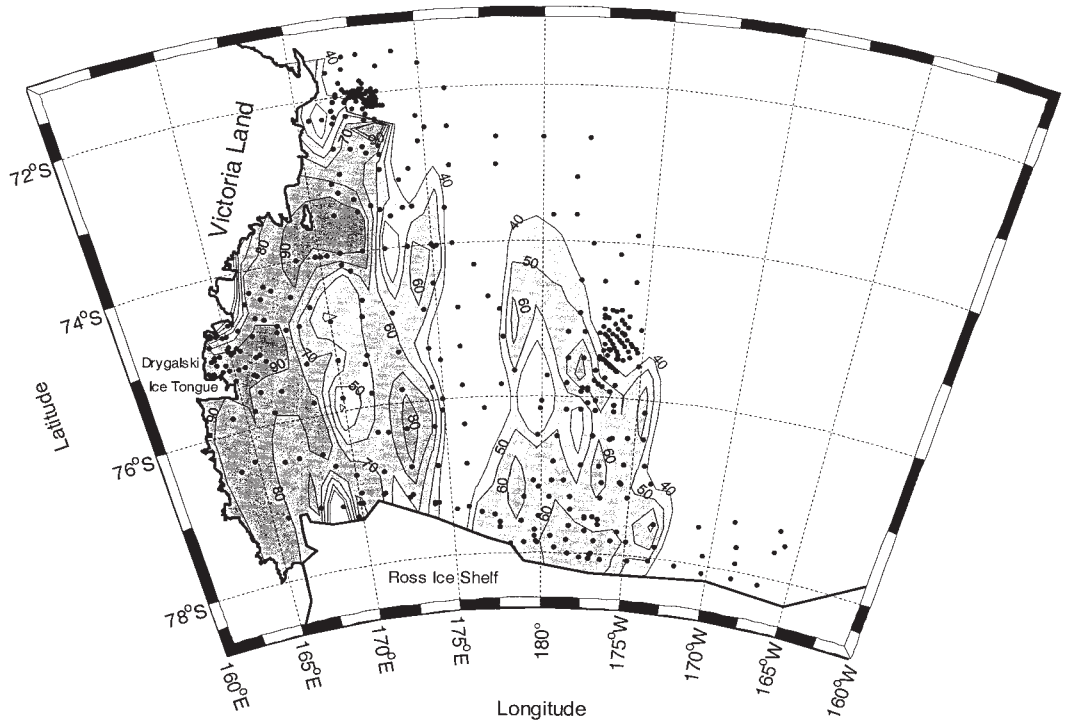

Fig. 6. OMP analysis solution at the sea bottom showing the HSSW contribution based on the complete dataset (summers 1994/95–2000/01).

Fig. 1). At a depth of 200 m, the intrusion of MCDW is evident, and is strongly modified by the interaction with the surrounding shelf waters. Because of its meandering path, the MCDW concentration does not show a continuous distribution, only some isolated peaks, as shown in Fig. 5a. Below the MCDW, the LSSW occupies an intermediate layer, with a thickness of about 200 m, which deepens near the RIS (Fig. 5b). In the deeper layer, the northward spreading DISW (Fig. 5c) flows over the thin layer of HSSW (Fig. 5d) which is in contact with the sea bottom, indicating that both sea water types are important elements in the hydrography of the continental slope in this region.

In order to emphasize the pathways of each water type, the OMP results have been represented at those depths

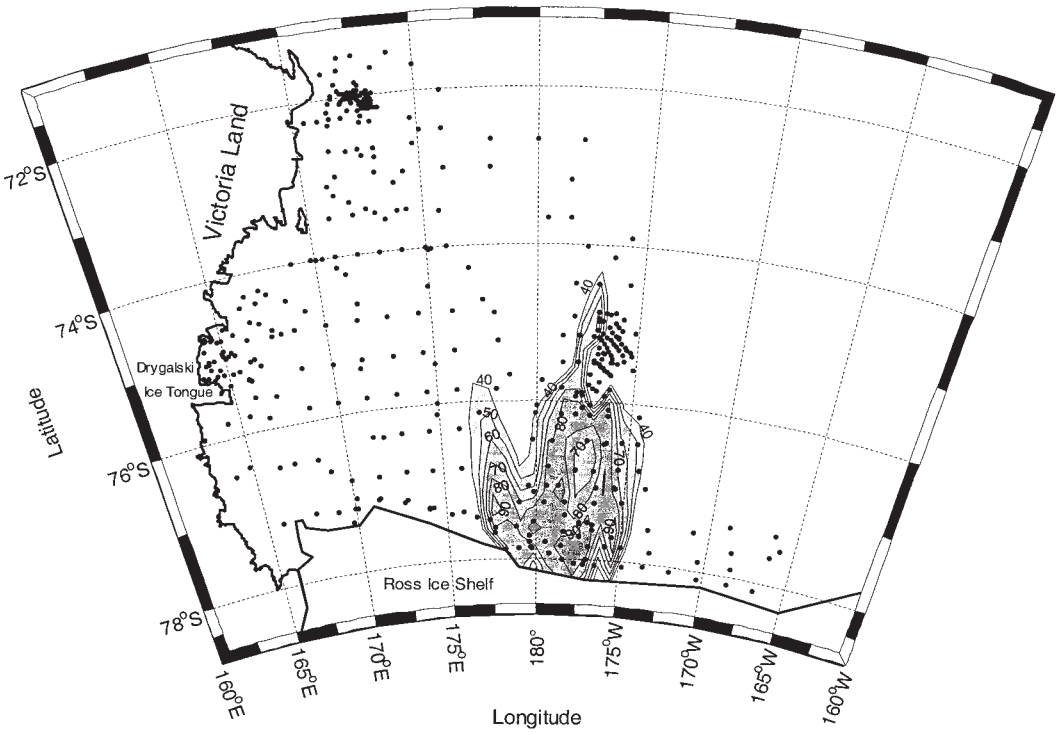

Fig. 7. OMP analysis solution at the minimum temperature surface showing the DISW contribution (depth varies between 350 and 500 m) based on the complete dataset (summers 1994/95–2000/01).

https://doi.org/10.1017/S095410200300110X Published online by Cambridge University Press

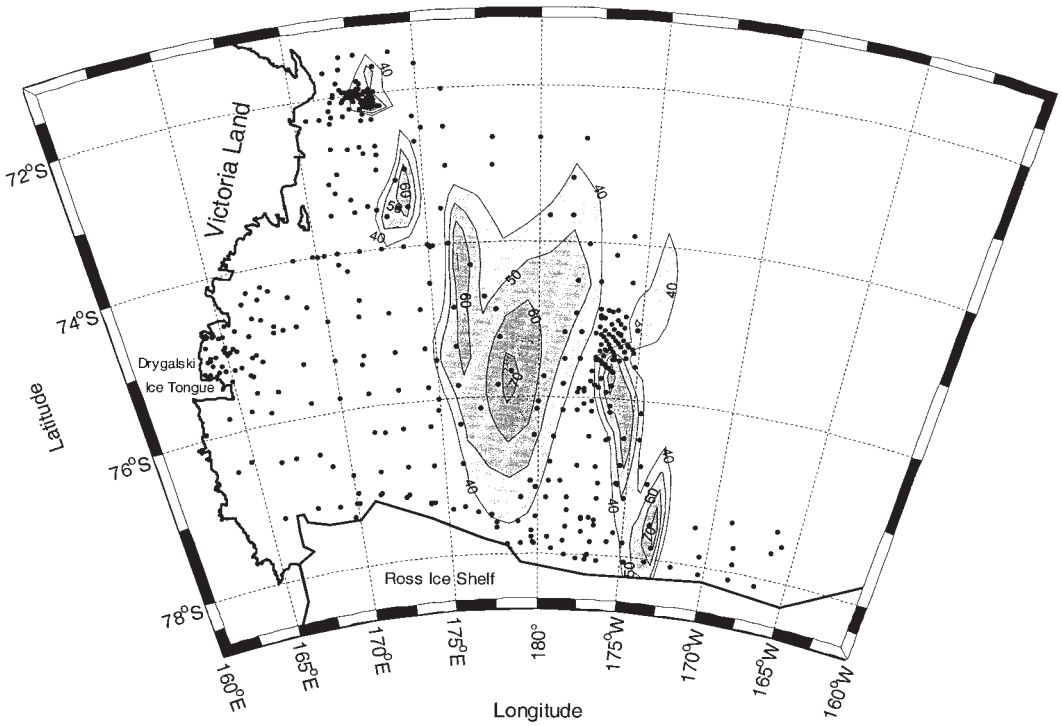

Fig. 8. OMP analysis solution at the maximum temperature surface showing the MCDW contribution (depth varies between 200 and 350 m) based on the complete dataset (summers 1994/95–2000/01).

where the maximum occurrence was expected. For this purpose the entire data set was used, merging the data collected from 1994/95 to 2000/01. This was necessary because the number of stations sampled during the individual surveys was insufficient to produce separate water mass distributions for the various years. During this period significant interannual variability was possible for some water masses. As inferred from Figs 3 & 4, some changes in the water mass structure are clear along the RIS. Combining such measurements into a single data set may introduce an unquantified spatial bias in the results, which is difficult to evaluate. Estimation of mean square errors for the computed water mass distribution would require a quantification of all bias and data errors. A similar technique

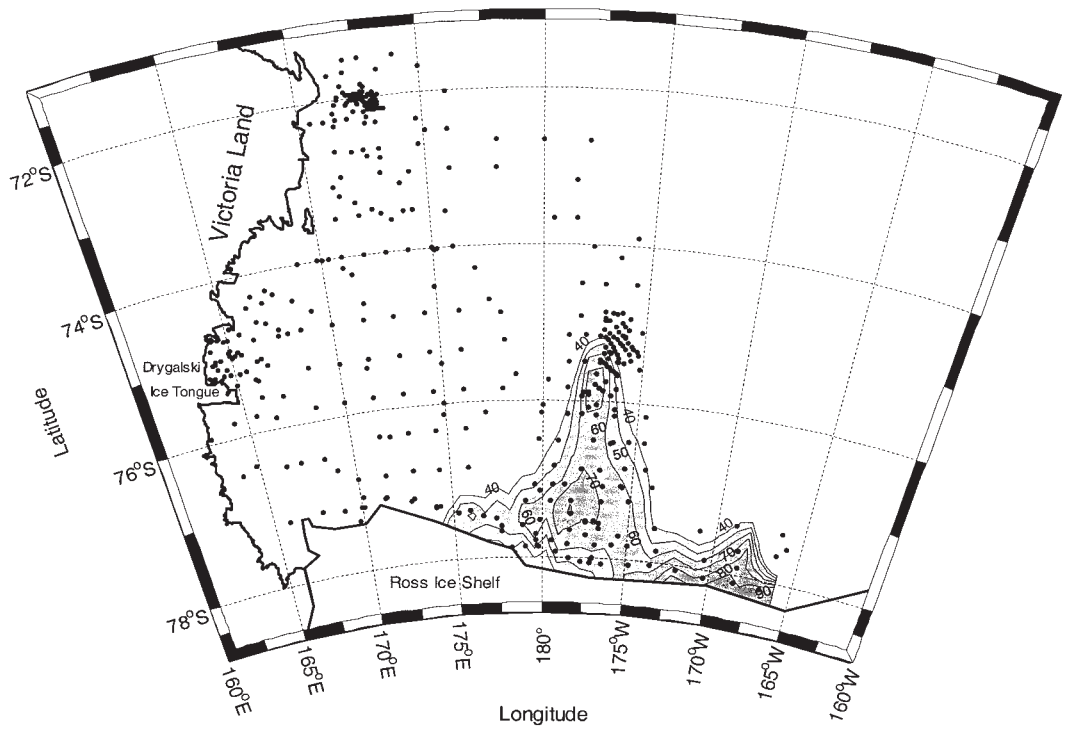

Fig. 9. OMP analysis solution at the surface showing the LSSW contribution (depth varies between 200 and 500 m, deepest values in the eastern sector) based on the complete dataset (summers 1994/95–2000/01).

https://doi.org/10.1017/S095410200300110X Published online by Cambridge University Press

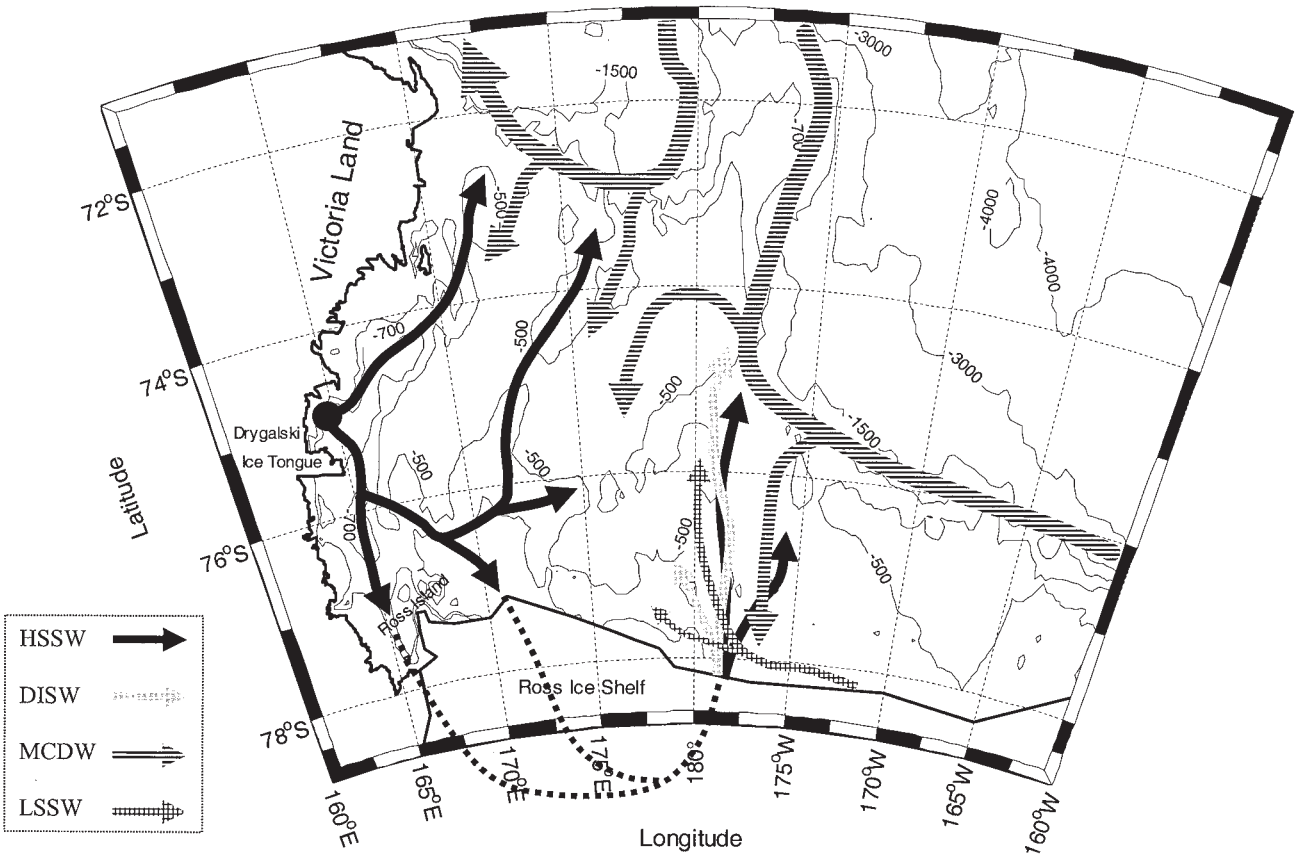

Fig. 10. A schematic diagram representing the subsurface circulation of the shelf waters in the Ross Sea region based on the OMP results.

has been used by some authors (e.g. Poole & Tomczak 1999, Hinrichsen & Tomczak 1993) who merged data collected during several decades with promising results. In particular the reader is referred to Hinrichsen & Tomczak (1993) for a more detailed assessment of errors inherent in OMP analysis when different data sets are combined together.

In the case of HSSW, which is the densest water in the Ross Sea (and in the Southern Ocean), the spreading was shown to occur in a layer close to the bottom (Fig. 6). The examination of the bottom layer indicates that the highest HSSW occurrence is found in the western sector of the Ross Sea where it has historically been observed (Jacobs *et al*. 1985). Eastward of 175°E, the HSSW contribution becomes small. It is noteworthy that the spread of HSSW has different intensities along the two directions of the Drygalski Basin, as evidenced by the different concentrations detected at the extremes of that basin. This indicates a dominant flow in the north-east direction, thus stressing the significant role that HSSW plays in the ventilation of the deep layers outside the western sector of the Ross Sea. The southward flow of HSSW bifurcates north of Ross Island (Fig. 6) at about 76.5°S. The eastern branch of the flow occupies the entire eastern basin and is stopped by Ross and Pennell banks at about 175°E. This means that high HSSW concentrations identified in the eastern sector are primarily due to intense spreading (driven by the bathymetry) of HSSW beneath the RIS. It stresses once more that HSSW plays a key role in the thermohaline circulation of the entire Ross Sea.

The DISW (Fig. 7) and the MCDW (Fig. 8) spreading were estimated respectively at the subsurface depth of minimum and maximum temperature. The non-horizontal distribution of DISW (its depth varies between 350 m, close to the RIS, to 500 m further north) indicates a main flow between 179W° and 176°W (Fig. 7). This flow reaches a latitude of 74.5°S, maintaining a percentage > 50%. Therefore the layer from a depth of 400 m to the bottom at the shelf break is essentially composed of HSSW and DISW (see also Figs 5c & d). This mixture most likely reaches the shelf break and takes part in the formation of the less saline bottom water (Jacobs *et al.* 1985). The DISW path illustrated by Figs 5d & 7 agrees with the experimental evidence reported by Budillon *et al*. (2002) as well as with the results shown in Rubino *et al*. (2003) which used a non-linear reduced gravity model.

The frontal zone at 177°W separates this water mass from the MCDW and the LSSW. Along the continental shelf

https://doi.org/10.1017/S095410200300110X Published online by Cambridge University Press

break, considerable southward penetrations of MCDW also occur at some specific locations. These intrusions, which are often located at the deepest depressions (> 500 m) of the continental shelf (see Fig. 1), are well illustrated by the MCDW concentration shown in Fig. 8 (see also Figs 3b, 4b & 5b).

Similarly the LSSW distribution is shown on the non-horizontal surface defined by the constraints: $34.47 < S < 34.52$, $-1.90 < \theta < -1.73$°C, $O_2 > 295$ µmol dm^{-3}. Consequently the results reported in Fig. 9 refer to depths varying from 200 to 500 m, with the deepest values observed in the eastern sector. Actually the LSSW reaches the bottom in the eastern sector (sea Fig. 3b) and becomes shallower in the western sector because of the presence of the denser HSSW. Moreover, the LSSW spreading also appears to be controlled by the MCDW intrusions, which form tongues of relatively warm water that prevent a further westward spreading of LSSW The distribution of water masses on the Ross Sea continental shelf suggests that this region is characterized by a complex water mass and frontal structure that varies over the entire study area. In order to simplify the interpretation of the results obtained in this study, a schematic diagram representing the most important pathways of the shelf waters is shown in Fig. 10. The more important results of this study include the strong dependency of the spreading path of water at different depth levels with the bathymetric structure of the area.

Conclusions

This work represents a regional application of the extended OMP analysis to studying the deep thermocline water mass distribution and circulation in the Ross Sea, based on an extensive dataset collected during four summer cruises between 1994/95 and 2000/01. To further constrain the analysis, we used Redfield ratios derived from field observations in the Ross Sea. This OMP analysis has provided a quantitative description of the water mass distribution in the area of interest, which was qualitatively validated by the identification of some "canonical" thermohaline characteristics.

In particular our results verify the extensive spreading of the HSSW over the western continental shelf and the important contribution it makes to the ventilation of the deep waters outside the Ross Sea. The intrusion of MCDW on to the continental shelf was identified and described. Finally a repeated section along the RIS revealed the thermohaline changes occurring during two successive summers.

The further knowledge contributed by recent field work should not, however, be taken to suggest that the hydrographical properties in the Ross Sea region are now perfectly understood.

With the increasing availability of hydrographical and chemical data in the Ross Sea, OMP can also be proposed as an objective method for characterizing the hydrographical features of that area, minimizing, in a statistical sense, the drawbacks that come from combining poorly intercalibrated datasets. The availability of a winter dataset would certainly allow a more complete definition of water mass distribution during the seasonal cycle.

The inclusion of data on suspended matter and chlorofluorocarbon tracer concentrations, which resolve the real age of each water mass, could further extend the application of OMP analysis in the Ross Sea. The ever expanding hydrographical data sets could possibly allow OMP analysis to be used in the study of seasonal and interannual variations in the distribution and circulation of water masses.

Acknowledgements

We thank the manuscript reviewers who helped to focus the discussion; in particular we thank Dr Victoria Cole who inspired Fig. 10 and the Guest Editor Dr M.L. Van Woert for his detailed suggestions. Figures 1 and 6–10 were produced utilizing the freeware *"m_map"* package software for MatLab® (http://www2.ocgy.ubc.ca/~rich/map.html). This study was performed as part of the Italian "National Program for Research in Antarctica" (PNRA: Programma Nazionale di Ricerche in Antartide) and was financially supported by ENEA through a joint research programme.

References

Alpkem. 1992a. Nitrate plus nitrite in seawater. *In The flow solution methodology*. *Document No. 000630, 8/92, Rev. B*. Wilsonville, OR: Alpkem, 19 pp.

Alpkem. 1992b. Orthophosphate in seawater. *In The flow solution methodology*. *Document No. 000626, 4/92, Rev. A*. Wilsonville, OR: Alpkem, 16 pp.

Alpkem. 1992c. Silica in seawater. *In The flow solution methodology*. *Document No. 000671, 4/92, Rev. A*. Wilsonville, OR: Alpkem, 16 pp.

Arrigo, K.R., Robinson, D.H., Worthen, D.L., Dunbar, R.B., Di Tullio, G.R., Van Woert, M. & Lizotte, M.P. 1999. Phytoplankton community structure and the drawdown of nutrients and CO_2 in the Southern Ocean. *Science,* **283**, 365–367.

Bromwich, D.H. & Kurtz, D.D. 1984. Katabatic wind forcing of the Terra Nova Bay polynya. *Journal of Geophysical Research*, **89**, 3561–3572.

Bergamasco, A., Defendi, V. & Meloni, R. 2002. Some dynamics of water outflow from beneath the Ross Ice Shelf during 1995/96. *Antarctic Science*, **14**, 74–82.

Budillon, G., Cordero Gremes, S. & Salusti, E. 2002. On the Dense Water Spreading off the Ross Sea shelf. *Journal of Marine Systems,* **35**, 207–227.

Budillon, G., Tucci, S., Artegiani, A. & Spezie, G. 1999. Water masses and suspended matter characteristics of the western Ross Sea. *In* Faranda, F.M., Guglielmo, L. & Ianora, A., *eds*. *Ross Sea ecology*. Berlin: Springer, 63–81.

Budillon, G., Fusco, G. & Spezie, G. 2000. A study of surface heat fluxes in the Ross Sea (Antarctica). *Antarctic Science*, **12**, 243–254.

Budillon, G. & Spezie, G. 2000. Thermohaline structure and variability in the Terra Nova Bay polynya, Ross Sea. *Antarctic Science*, **12**, 493–508.

https://doi.org/10.1017/S095410200300110X Published online by Cambridge University Press

CATALANO, G., BENEDETTI, F., PREDONZANI, S., GOFFART, A., RUFFINI, S., RIVARO, P. & FALCONI, C. 1999. Spatial and temporal patterns of nutrient distributions in the Ross Sea *In* FARANDA, F.M., GUGLIELMO, L. & IANORA, A., *eds*. *Ross Sea ecology*. Berlin: Springer, 107–120.

CATALANO, G., POVERO, P., FABIANO, M., BENEDETTI, F. & GOFFART, A. 1997. Nutrient utilization and particulate organic matter changes during summer in the upper mixed layer (Ross Sea, Antarctica). *Deep-Sea Research*, **44**, 97–112.

EL-SAYED, S.Z. & TAGUCHI, S. 1981. Primary production and standing crop of phytoplankton along the ice-edge in the Weddell Sea. *Deep-Sea Research*, **28**, 1017–1032.

EPPLEY, R.W. & PETERSON, B.J. 1979. Particulate organic fluxes and planktonic new production in the deep ocean. *Nature*, **282**, 677–680.

FUSCO, G., FLOCCO, D., BUDILLON, G., SPEZIE, G. & ZAMBIANCHI, E. 2003. Dynamics and variability of Terra Nova Bay Polynya. *Marine Ecology PSZNI*.

GORDON, L.I., CODISPOTI, L.A., JENNINGS JR, J.C., MILLERO, F.J., MORRISON, J.M. & SWEENEY, C. 2000. Seasonal evolution of hydrographical properties in the Ross Sea, Antarctica 1996–1997. *Deep-Sea Research*, **47**, 3095–3117.

GORDON, A.L. & TCHERNIA, P. 1972. Waters of the continental margin off Adélie coast, Antarctica. *Antarctic Research Series*, **19**, 56–69.

GOURETSKI, V. 1999. The large-scale thermohaline structure of the Ross Gyre. *In* SPEZIE, G. & MANZELLA, G.M.R., *eds. Oceanography of the Ross Sea, Antarctica*. Berlin: Springer, 77–100.

GROTTI, M., SOGGIA, F., ABELMOSCHI, M.L., RIVARO, P., MAGI, E. & FRACHE R. 2001. Temporal distribution of trace metals in Antarctic coastal waters. *Marine Chemistry*, **76**, 189–209.

HANSEN, H.P. & GRASSHOFF, K. 1983. Automated chemical analysis. *In* GRASSHOFF, K., EHRHARDT, M. & KREMLING, K., *eds. Methods of seawater analysis*. Weinheim: VCh, 347–379.

HINRICHSEN, H. & TOMCZAK, M. 1993. Optimum multiparameter analysis of water mass structure in the western North Atlantic Ocean. *Journal of Geophysical Research*, **98**, 10 155–10 169.

IANNI, C., RIVARO, P. & FRACHE, R. In press. Distribution of dissolved and particulate iron, copper and manganese in the shelf waters of the Ross Sea (Antarctica). *Marine Ecology PSZNI*.

JACOBS, S.S., AMOS, A.F. & BRUCHHAUSEN, P.M. 1970. Ross Sea oceanography and Antarctic Bottom Water formation. *Deep-Sea Research*, **17**, 935–962.

JACOBS, S.S. & COMISO, J.C. 1989. Sea ice and oceanic processes on the Ross Sea continental shelf. *Journal of Geophysical Research*, **94**(C12), 18 195–18 211.

JACOBS, S.S., FAIRBANKS, R.G. & HORIBE, Y. 1985. Origin and evolution of water masses near the Antarctic continental margin: evidence from $H_2{}^{18}O/H_2{}^{16}O$ ratios in seawater. *Antarctic Research Series*, **43**, 59–85.

JACOBS, S.S. & GIULIVI, C.F. 1998. Interannual ocean and sea ice variability in the Ross Sea. *Antarctic Research Series*, **75**, 135–150.

JACOBS, S.S. & GIULIVI, C.F. 1999. Thermohaline data and ocean circulation on the Ross Sea continental shelf. *In* SPEZIE, G. & MANZELLA, G.M.R., *eds. Oceanography of the Ross Sea, Antarctica*. Berlin: Springer, 3–16.

JACOBS, S.S., GIULIVI, C.F. & MELE, P.A. 2002. Freshening of the Ross Sea during the late 20th century. *Science*, **297**, 386–389.

JACOBS, S.S., GORDON, A.L. & ARDAI JR, J.L. 1979. Circulation and melting beneath the Ross Ice Shelf. *Science*, **203**, 439–442.

JENNINGS JR, J.C., GORDON, L.I. & NELSON, D.M. 1984. Nutrient depletion indicates high primary productivity in the Weddell Sea. *Nature*, **309**, 51–54.

KARTENSEN, J. & TOMCZAK, M. 1998. Age determination of mixed water masses using CFC and oxygen data. *Journal of Geophysical Research*, **103**(C9), 18 599–18 609.

KURTZ, D.D. & BROMWICH, D.H. 1983. Satellite observed behavior of the Terra Nova Bay polynya. *Journal of Geophysical Research*, **88**, 9717–9722.

KURTZ, D.D. & BROMWICH, D.H. 1985. A recurring atmospherically-forced polynya in Terra Nova Bay. *Antarctic Research Series,* **43**, 177–201.

LOCARNINI, R.A. 1994. *Water masses and circulation in the Ross Gyre and environs*. PhD thesis, Texas A&M University, 87 pp. [Unpublished]

LE JEHAN, S. & TREGUER, P. 1985. The distribution of inorganic nitrogen, phosphorus, silicon and dissolved organic matter in surface and deep water of the Southern Ocean. *In* SIEGFRIED, W.R., CONDY, P.R. & LAWS, R.M., *eds. Antarctic nutrient cycles and food web*. Berlin: Springer, 22–29.

LIPIZER, M., RUFFINI, S., PREDONZANI, S., COZZI, S., GOFFART, A. & CATALANO, G. 1997. Antarctic spring: the importance of "new" production. *Proceedings XII Congresso Associazione Italiana di Oceanologia e Limnologia, 18–21 September 1996, Isola di Vulcano*, **1**, 153–163.

LIPIZER, M., MANGONI, O., CATALANO, G. & SAGGIAMO, V. 2000. Phytoplankton uptake of ^{15}N and ^{14}C in the Ross Sea during austral spring 1994. *Polar Biology*, **23**, 495–502.

MACKAS, D.L., DENMAN, K.L. & BENNETT, A.F. 1987. Least square multiple tracer analysis of water mass composition. *Journal of Geophysical Research*, **92**(C3), 2907–2918.

NELSON, D.M. & SMITH, W.O. 1986. Phytoplankton bloom dynamics of the western Ross Sea ice edge 2. Mesoscale cycling of nitrogen and silicon. *Deep-Sea Research*, **33**, 1389–1412.

POOLE, R. & TOMCZAK, M. 1999. Optimum Multiparameter analysis of the water mass structure in the Atlantic Ocean thermocline. *Deep-Sea Research*, **46**, 1895–1921.

REDFIELD, A.C., KETCHUM, B.H. & RICHARDS, F.A. 1963. The influence of organisms on the composition of sea-water. *In* HILL, M.N., *ed. The Sea. Wiley-Interscience*, **2**, 26–77.

RODMAN, M. & GORDON, A. 1982. Southern Ocean bottom waters in the Australia-New Zealand sector. *Journal of Geophysical Research*, **87**, 5771–5778.

RUBINO, A., BUDILLON, G., PIERINI, S. & SPEZIE, G. 2003. A model for the spreading and sinking of the Deep Ice Shelf Water in the Ross Sea. *Antarctic Science*, **15**, 25–30.

RUSSO, A. 1999. Water mass characteristics during the ROSSMIZE Cruise (western sector of the Ross Sea, November–December 1994). *In* SPEZIE, G. & MANZELLA, G.M.R., *eds. Oceanography of the Ross Sea, Antarctica*. Berlin: Springer, 83–93.

SAGGIOMO, V., CATALANO, G., MANGONI, O., BUDILLON, G. & CARRADA, G.C. 2002. Primary production in ice-free waters of the Ross Sea (Antarctica) during the austral summer 1996. *Deep-Sea Research,* **49**, 1787–1801.

STRICKLAND, J.D.H. & PARSONS, T.R. 1972. A practical handbook of sea water analysis. *Bulletin of the Fisheries Research Board of Canada*, No. 167, 1–311.

TOMCZAK, M. 1981. A multiparameter extension of temperature/salinity diagram techniques for the analysis of *non*-isopycnal mixing. *Progress in Oceanography*, **10**, 147–171.

TOMCZAK, M. 1999. Some historical, theoretical and applied aspects of quantitative water mass analysis. *Journal of Marine Research,* **57**, 275–303.

TOMCZAK, M. & LARGE, D.G.B. 1989. Optimum Multiparameter analysis of mixing in the thermocline of the eastern Indian Ocean. *Journal of Geophysical Research*, **94**(C11), 16141–16149.

TRUMBORE, S.E., JACOBS, S.S. & SMETHIE JR, W.M. 1991. Chlorofluorocarbon evidence for rapid ventilation of the Ross Sea. *Deep-Sea Research*, **38**, 845–870.

UNESCO 1983. The acquisition, calibration and analysis of CTD data. A report of SCOR WG 51. *Technical Papers in Marine Science*, **54**, 1–59.

UNESCO 1988. Algorithms for computation of fundamental properties of seawater. *Technical Papers in Marine Science*, **44**, 1–53.

VAN WOERT, M.L. 1999. Wintertime dynamics of the Terra Nova Bay polynya. *Journal of Geophysical Research,* **104**(C49), 7753–7769.